Modeling of Plasma Current Decay during Disruptions Caused by Massive Impurity Injection*)

Hirokazu OHWAKI, Masayoshi SUGIHARA[1)] and Akiyoshi HATAYAMA

Keio University, Yokohama 223-8522, Japan

[1)]*ITER International Team, Naka JWS, Naka 311-0193, Japan*

(Received 14 March 2005 / Accepted 20 January 2006)

A numerical model is developed to evaluate the decay time of plasma current during the disruption following intense impurity injections. Our model is based on the power balance equation between joule heating and impurity radiation as a way to evaluate the electron temperature and charge state after the thermal quench. The model is applied to the experimental results of massive N_2 gas injections in JFT-2M, which simulate the "ingress-of-coolant event" (ICE) as well as disruption mitigations in ITER. It is confirmed that the model can reproduce the experiments reasonably well.

Keywords: disruption, current decay time, impurity radiation, mitigation, tokamak

DOI: 10.1585/pfr.1.016

1. Introduction

There is a pressing need to enhance the robustness of the vacuum vessel and in-vessel components of ITER against the various deleterious effects of disruptions, namely (i) heat loads during thermal quench, (ii) electromagnetic (EM) forces due to induced eddy and halo currents during current quench, and (iii) runaway electron generation and its damping to the wall. For this purpose, a robust design and the simultaneous amelioration of these deleterious effects are essential. The large halo current induced during a vertical displacement event (VDE) with a slow current quench is most important in regard to the vacuum vessel. On the other hand, the eddy current induced during a fast current quench is essential for the in-vessel components [1]. These two currents generate the EM loads by interaction with the magnetic field, and these loads could be large enough to break the vacuum vessel and in-vessel components mechanically. For example, it is believed that three carbon tiles in the first wall were broken by the EM force due to the halo current during the disruption in JT-60U [2]. A fast current quench also tends to generate runaway electrons owing to the increase of the loop voltage induced by a combination of the current decay and the avalanche effect [3].

The prevention of VDEs leads to the suppression of the EM load caused by the halo current. In JT-60U, the avoidance of VDEs and plasma-wall interaction has been achieved by controlling the plasma current center and equilibrium [4, 5], which is called a neutral point (NP). This suggests the possibility that VDEs might be avoidable by employing the NP of the plasma current center. Since there is no universal NP [6], however, the halo current should be decreased during a VDE, in particular caused by a slow current quench. In DIII-D, a reduction of the halo current was observed by shutting down the plasma very quickly by means of a massive impurity injection [7]. This indicates that a fast plasma shutdown can reduce the halo current. A variety of fast plasma shutdown scenarios, e.g., the active injection of neutral species such as a noble gas pellet [8], liquid deuterium [9], or impurity-doped deuterium pellets [10], have been proposed. It has been shown, however, that the injection of impurities involving pellets easily leads to runaway generation due to the avalanche effect [11]. In present day tokamaks, runaway electrons are frequently observed following the injection of impurities [12]. The suppression of runaways can be effectively achieved by increasing the electron density [3, 13], decreasing the current quench rate and effective safety factor [14], and employing magnetic turbulence [15]. In some experiments, the disappearance of runaways and decreases of the heat flux to the divertor have been realized by large impurity injections [16, 17]. Hence, the introduction of large quantities of impurities appears to be favorable for suppression of the heat load, halo current, and runaway generation. In fact, several experiments aimed at mitigating disruption effects (e.g., heat fluxes to the divertor plates, runaway electrons) have involved the introduction of large impurity gases [7, 18].

In order to suppress the EM load induced by the eddy current, it is essential to reduce the current quench rate by decreasing impurity influxes into the core plasma during thermal quench [13]. This indicates that an intense impurity injection can be harmful for this purpose. In contrast, a

author's e-mail: akh@ppl.appi.keio.ac.jp

*) This work has been partly performed while the first author (H. O.) was staying at Japan Atomic Energy Agency (Mukaiyama, Naka-shi, Ibaraki-ken, Japan)

reduction of the current decay rate in Tore Supra has been achieved by means of a massive helium injection [18], which suggests that the current decay time depends also on the type of injected impurities as well as the amount of them. These dependencies have not yet been clearly understood. Thus, in this paper, we will present a simple numerical model, which can evaluate the current quench time during a disruption as a function of the amount of various injected impurity species. This model is compared with experiments involving intense injections of nitrogen gas demonstrated in JFT-2M [19], which simulate the ingress-of-coolant event (ICE) as well as the disruption mitigation in ITER.

In the model, the decay time of the plasma current is estimated based on the L/R time, where L is the self-inductance and R is the plasma resistance. This L/R time is primarily determined by the plasma resistance R after the thermal quench. Therefore, it is essential to properly evaluate the electron temperature and effective charge after the thermal quench. The electron collisions with neutrals might contribute significantly to the resistance, especially in cases of massive impurity injection. Other effects can also influence the L/R time, i.e., changes of the plasma equilibrium configuration during the current quench. A rigorous treatment of these effects requires a detailed disruption simulation code, such as DINA [20] or TSC [21]. This important issue, however, will be left for future study and will not be discussed in the present paper.

During the current quench phase, the impurity content is usually very high, so that the dominant energy loss channel is the radiation from impurities, while the ordinary transport loss and auxiliary heating are comparatively very small. This radiation loss is then balanced with the joule heating converted from the magnetic energy of the plasma current, which results in the fast plasma current decay. Thus, detailed evaluations of the impurity radiation, charge state, and densities of hydrogen and impurities are of primary importance. These detailed processes are very complicated and a sophisticated numerical code will be necessary to fully evaluate such processes. Several codes, e.g., KPRAD [22], have been developed for this purpose. Such codes, however, are fairly complicated and may not be relevant for a wide range of parameter studies in terms of impurity content and pre-disruptive plasma conditions, etc. This paper describes the development of a much simpler numerical model to estimate the balanced condition between the radiation of impurities and joule heating. This simple model will also be quite effective when we incorporate this balanced process into a detailed disruption simulation code, DINA or TSC, which is required for more comprehensive and sophisticated examinations of plasma disruption.

The paper is organized as follows. In Sec. 2, the numerical model for the decay time of the plasma current, the plasma resistivity, and the power balance between the impurity radiation and the joule heating is described. In Sec. 3, comparisons of the developed model with gas injection experiments performed in JFT-2M are presented. Sec. 4 presents a summary of the conclusions.

2. Numerical Model

2.1 Plasma current decay time

During the current quench phase, the plasma current decays freely with its resistive time scale which can be expressed by the following simple circuit equation,

$$RI_{\mathrm{p}} + \frac{\mathrm{d}}{\mathrm{d}t}\left(LI_{\mathrm{p}}\right) = V_{\mathrm{ex}}, \tag{1}$$

where I_{p} is the plasma current. The externally applied voltage V_{ex} can affect the behavior of the current decay during disruptions, especially for disruptions having a slow current decay. When the intrinsic current decay is slow, which may be caused by a small impurity influx during the thermal quench, the induced loop voltage due to the plasma current decay is small. In this case, the plasma current decay can be slowed down significantly and sustained or even recovered to its original level by applying the external voltage within the capability of the power supply. This might be one of the reasons for the large scatter of the current decay times of the existing devices, which are indicated in the disruption database [23]. In the case of a disruption having a fast current decay, however, the external voltage is usually much smaller than the loop voltage induced due to the plasma current decay (second term in the left-hand side of Eq. (1)). In this case, the external voltage will have little effect on the behavior of the current decay. For instance, in JFT-2M machine, which is examined later in this paper, the maximum voltage of the thyristor power supply for the ohmic coil system is $\approx$ 600 V [24]. The number of turns in this coil ranges from 42 (circular plasma) to 84 (D-shaped plasma) [24]. Thus, the available one-turn voltage is in the range of 7–14 V. This voltage measured particularly at the plasma surface is still reduced due to the vacuum vessel's shielding effect when the current decay time is comparable or shorter than the vacuum vessel's time constant. In a representative case, the induced loop voltage during the fast current decay examined in this paper is $\approx$ 450 V, with $L \approx 3\,\mu$H, $I_{\mathrm{p}} \approx 150$ kA, and a decay time of $\approx$ 1 ms, which is an order of magnitude larger than the maximum available voltage from the ohmic coil. This characteristic becomes more remarkable in large devices for future development, such as ITER, equipped with superconducting magnets, in which the external voltage is greatly limited due to the voltage limitation of the superconducting magnets and the power supply. Actually, in the case of ITER for example, a maximum of only $\approx$ 10 V can be externally applied, whereas the induced loop voltage during a fast current quench is expected to be $\approx$ 2–3 kV. Since in this paper we will concentrate on the disruptions having a fast current decay caused by a large impurity influx, we will omit the external voltage in the right-hand side of Eq. (1). As mentioned above, this omission is not

always valid. For the analysis of disruptions with a slow current decay or disruptions in other devices having larger power supply systems, the external voltage must be properly taken into account.

From Eq. (1) with $V_{ex} = 0$, we obtain the following simple solution if R and L are constant,

$$I_p = I_{p0} \exp\left(-\frac{t}{\tau_c}\right), \tag{2}$$

$$\tau_c = \frac{L}{R}, \tag{3}$$

where I_{p0} is the plasma current before the current quench, and τ_c is the time constant of I_p decay. Thus, the current decay time can be approximated by $\tau_c = L/R$ with the assumption that L and R are constant during the current quench phase for simplicity.

2.2 Plasma resistivity

Plasma resistance is represented by plasma resistivity η which includes the Coulomb collision (Spitzer resistivity) and the collision between electrons and neutral particles (rigid body collision),

$$R = \frac{2\pi R_m \eta}{\pi \kappa a^2}, \tag{4}$$

$$\eta = \frac{m_e v_e}{n_e e^2} \sum n\sigma = 5.22 \times 10^{-5} \frac{Z_{eff} \ln \Lambda}{T_e^{3/2}} + 1.49 \times 10^{13} \frac{T_e^{1/2}}{n_e} \left(n_H^0 \pi {d_H}^2 + n_z^0 \pi {d_z}^2\right), \tag{5}$$

$$Z_{eff} = \frac{n_H^i + \sum_{k=1}^{K} k^2 n_z^k}{n_e}, \tag{6}$$

where R_m and a are the major and minor radii, respectively, κ is the plasma elongation, m_e is the mass of electrons, v_e is the electron velocity, e is the elementary charge, σ is the collisional cross-section, Z_{eff} is the effective charge, $\ln \Lambda$ is the Coulomb logarithm, and T_e is the electron temperature. In addition, n_e, n_H^0, n_z^0, n_H^i, and n_z^k are the densities of electrons, neutral hydrogen, neutral impurities, protons, and impurity ions of the k-th charge state, respectively. Here we employ the simple rigid body model for collisions between electrons and neutrals. Then, d_H and d_z are the atomic radii of hydrogen and impurities, respectively. By comparing the first term with the second and third terms of Eq. (5), it is easily understood that the Coulomb collision dominates the resistivity in the case of ordinary massive impurity injections ($n_z^0 < 10^{22}\,\mathrm{m}^{-3}$, $T_e \sim 1\,\mathrm{eV}$). The contribution of neutral particles becomes significant when neutral particles are about one hundred times as large as ions (as in the case of extremely massive injections). Thus, the most essential parameter in determining the resistivity is the electron temperature T_e for a given impurity content, since the impurities' charge state and consequently Z_{eff} are determined by T_e.

For the Coulomb logarithm, the following expression is used, in which T_e is in keV and n_e is in $10^{20}\,\mathrm{m}^{-3}$ [25].

$$\ln \Lambda = \begin{cases} 17.2 + \ln\left(T_e^{3/2} / \left(n_e^{1/2} Z_{eff}\right)\right), & T_e < 0.01 {Z_{eff}}^2, \\ 14.8 + \ln\left(T_e / n_e^{1/2}\right), & T_e > 0.01 {Z_{eff}}^2. \end{cases} \tag{7}$$

2.3 Power balance

In this paper, for the sake of simplicity we assume coronal equilibrium after the thermal quench. The densities of each charge state of hydrogen and impurities, which are important parameters for the resistivity, are taken from the ADAS package [26] in which the ion ratios of each charge state are tabulated as a function of T_e. Here the ion ratio is defined as a ratio of the density of each charge state to the total density including neutrals. These ratios vary somewhat with changes in the electron density n_e. Figures 1 (a), (b), and (c) show the ion ratios in the case of nitrogen impurity for the electron densities of 10^{19}, 10^{20}, and $10^{21}\,\mathrm{m}^{-3}$, respectively. It is seen from these figures that the density dependence is very weak in the density range considered in this paper, i.e., $10^{19} < n_e < 10^{22}\,\mathrm{m}^{-3}$. Accordingly, we use the ion ratios for $n_e = 10^{20}\,\mathrm{m}^{-3}$ as a typical electron density in the present calculations.

During the current quench phase, it is expected that both the auxiliary heating and ordinary transport loss powers are negligibly small compared to the joule heating and radiative loss powers. Thus, the joule heating power density (P_{joule}) can be equated to the radiative loss one (P_{rad}),

$$P_{joule}(T_e) = P_{rad}(T_e). \tag{8}$$

The joule heating and radiative loss power densities are expressed as

$$P_{joule}(T_e) = \eta(T_e)\, j^2, \tag{9}$$

$$P_{rad}(T_e) = n_e(T_e) \sum_{k=0}^{K} n_z^k(T_e)\, L_z^k(T_e) = n_e(T_e)\, n_z^{total} L_z^{total}(T_e), \tag{10}$$

where j is the plasma current density, L_z^k is the emissivity for the impurity of the k-th charge state, n_z^{total} is the total impurity density including neutrals, and L_z^{total} is the total emissivity in coronal equilibrium. In Eq. (10), the total emissivity L_z^{total} is tabulated as a function of T_e in the ADAS as shown in Fig. 2 for the electron densities of 10^{19}, 10^{20}, and $10^{21}\,\mathrm{m}^{-3}$. It is seen from the figure that the density dependence is very weak for the temperature range $T_e < 10\,\mathrm{eV}$, which is of primary interest in the present investigation. Thus, we use the emissivity curve for $n_e = 10^{20}\,\mathrm{m}^{-3}$.

As shown in Fig. 3, P_{joule} and P_{rad} are strongly dependent on T_e for two different total nitrogen densities. The device parameters used in this calculation are taken from JFT-2M as shown later. Both power densities balance at a certain T_e determined by Eq. (8) for a given total impurity density. Finally, we can determine the plasma resistance after the thermal quench and evaluate the L/R time using an estimated value of L.

The parameters of JFT-2M used in the calculations are as follows: $R_m = 1.31\,\mathrm{m}$, $a = 0.28\,\mathrm{m}$, $\kappa = 1.4$,

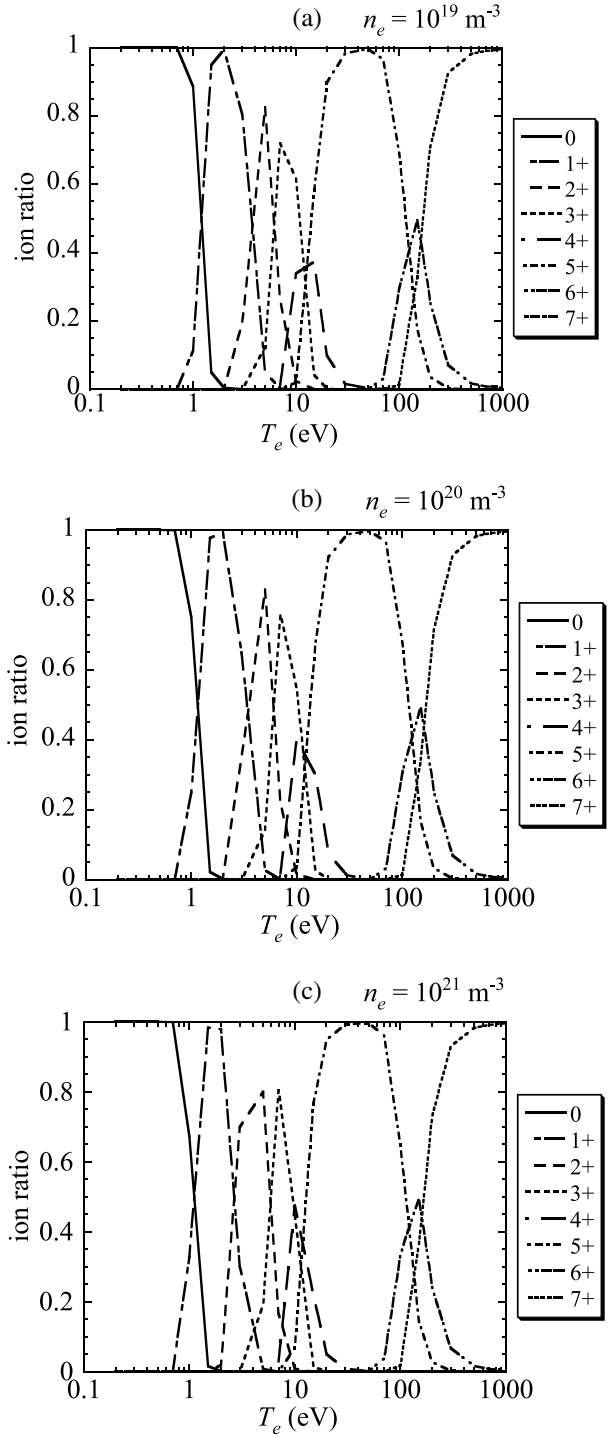

Fig. 1 The ion ratios of each nitrogen charge state as a function of T_e for (a) $n_e = 10^{19}$, (b) 10^{20}, and (c) 10^{21} m^{-3} taken from Ref. [26]. A very weak dependence on the electron density is seen.

$I_{p0} = 150$ kA, $L = 3\,\mu$H, and $n_H^{total} = 3 \times 10^{19}$ m^{-3} (n_H^{total} is the total hydrogen density including neutrals). In the model, hydrogen and impurity densities are determined by the ion ratios as shown in this section. Therefore, we assume implicitly that all the injected particles are absorbed into the plasma and are in a coronal equilibrium state instantaneously.

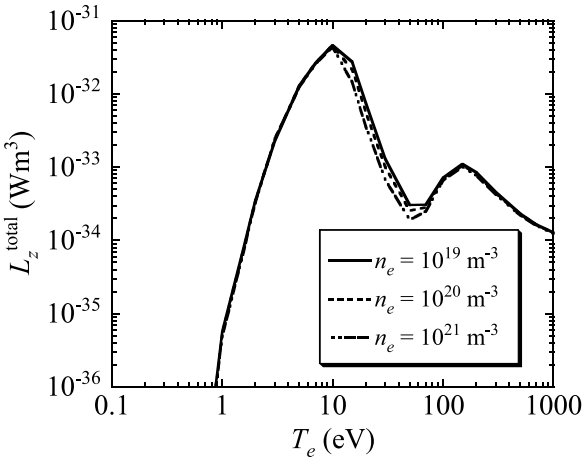

Fig. 2 The total emissivity L_z^{total} of nitrogen for $n_e = 10^{19}$, 10^{20}, and 10^{21} m^{-3} [26]. The emissivity curves are quite similar for these densities in $T_e < 10$ eV.

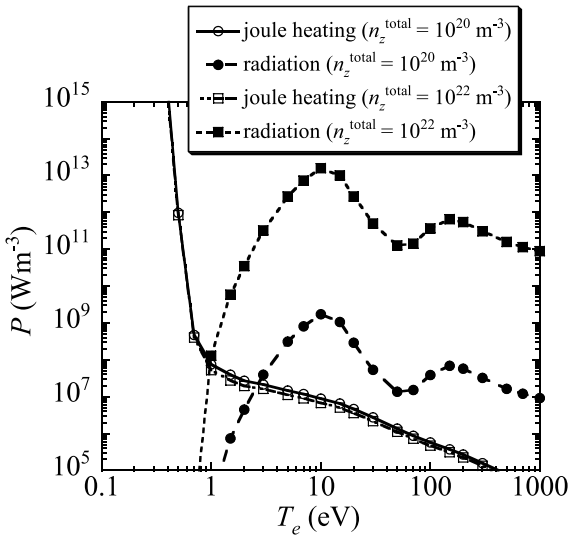

Fig. 3 Dependences of P_{joule} and P_{rad} on T_e for $n_z^{total} = 10^{20}$ m^{-3} (open and closed circles) and 10^{22} m^{-3} (open and closed squares), respectively. Calculations are done using JFT-2M tokamak parameters.

3. Comparison with Experiments

In JFT-2M, experiments involving the injection of nitrogen gas have been performed to simulate the ICE as well as disruption mitigations in ITER. One of these experiments is shown in Fig. 4. The solid and dashed lines indicate the experimental waveform of the plasma current and exponential curve having the decay constant $\tau_c = 1.1$ ms, respectively. Details of the experimental setup and the experimental results are presented in Ref. [19]. In these experiments, a rupture disk (RD) has been used to realize quick injections of gas. In addition, at the downstream of

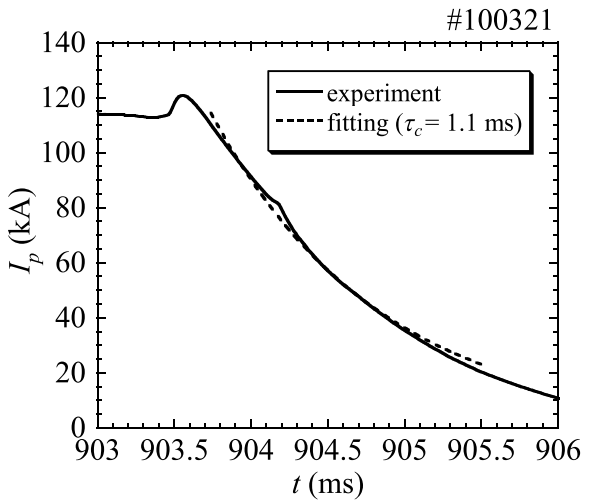

Fig. 4 Current waveform experimentally obtained (solid line) [19]. The exponential fitted curve with τ_c = 1.1 ms is also shown by a dashed line.

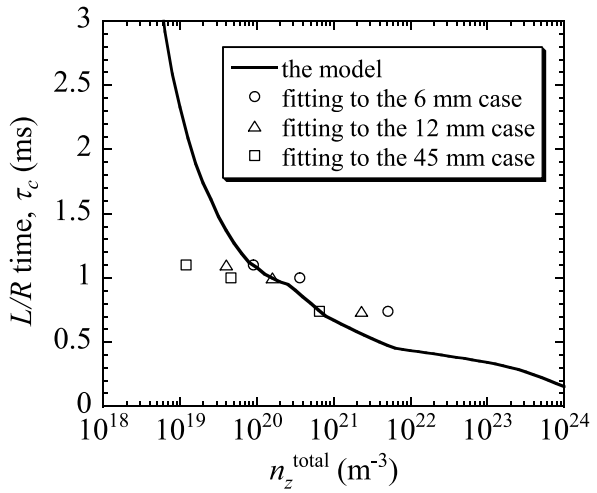

Fig. 5 The L/R time calculated with the present model (solid line) and τ_c observed in JFT-2M experiments [19] (open circles, triangles, and squares) as a function of n_z^{total}, which is the sum of nitrogen atoms and ions contributing to the disruption.

the RD, orifices of different diameters (6, 12, and 45 mm) have been used to control the amount of the injected impurity gas. The current decay times τ_c for each RD have been fitted with an exponential curve using 80% to 20% of I_{p0} (cf. Fig. 4), which is a reasonable way to evaluate the EM force induced by the eddy current and which is recommended in Ref. [23]. Thus, a comparison of the present model with these experiments provides an effective way to check the validity of the model. Unfortunately, the absolute amount of the injected impurity has not been directly measured in these experiments, and only an estimation has been provided based on the gas pressure gauge. This estimation, however, is not simple since it involves several uncertainties, e.g., a detailed time sequence of the rupture of the RD and the gas speed through the rupture of the RD. These uncertainties can easily alter the estimation of the injected amount by more than an order of magnitude, i.e., the typical range becomes 10^{19}–10^{21} m^{-3}, which makes the comparison unclear. Thus, in the present paper, we will compare the modeling results to the experimental τ_c using the relative amount of injected gas by simply assuming that the injected amount is proportional to the area of each orifice.

Figure 5 shows the calculated L/R time (solid line) and the experimental τ_c (open circles, triangles, and squares) as a function of n_z^{total}. The open circles show the case in which the injected amount is adjusted to provide the same current quench time for the experiment (τ_c) and the calculation (the L/R time) using a 6 mm orifice, while the injected amounts for 12 mm and 45 mm orifices are increased proportionally to each of their areas. In a similar way, open triangles and squares correspond to the cases in which the injected amounts are adjusted to provide the same current quench times for 12 and 45 mm orifices, respectively, while the injected amounts used in cases involving other diameter orifices are increased or decreased proportionally to each of their orifices. It is seen from this comparison that the global feature of the reduction of τ_c with increases in the amount of injected impurity can be reproduced reasonably well using the present model.

It is noticed in Fig. 5 that the reduction of the L/R time becomes very slight with an increase of n_z^{total} from $n_z^{total} \approx 10^{20}$ m^{-3}. This behavior is due to the proportionality of the plasma resistivity to $T_e^{-3/2}$ and Z_{eff}. In this region, the reduction of T_e is compensated by that of Z_{eff}, as is clearly seen in Fig. 6. The effective charge Z_{eff} increases with an increase of the impurity's ion density up to $n_z^{total} \approx 10^{19}$ m^{-3}, and then starts to decrease due to decreases of the impurity density at a high charge state ($k \geq 2$). The discontinuity in the Z_{eff} curve around $n_z^{total} = 2 \times 10^{19}$ m^{-3} is due to the simple linear interpolation of sparse data points for the ion ratios in the ADAS code. The electron collisions with neutrals produce a large contribution to the resistivity in $n_z^{total} > 10^{23}$ m^{-3} (Fig. 7). In extremely massive impurity injections, the role of neutral particles in the plasma resistivity becomes significant.

4. Conclusions

We have developed a simple numerical model to evaluate the plasma current decay time for a given amount of total impurity density. The model is based on the power balance between the joule input and the radiation loss, using the plasma resistivity including collisions between electrons and neutral particles. The model is compared with the current decay times observed in JFT-2M disruption experiments using a massive nitrogen injection. It is shown that the decrease of the current decay time with the

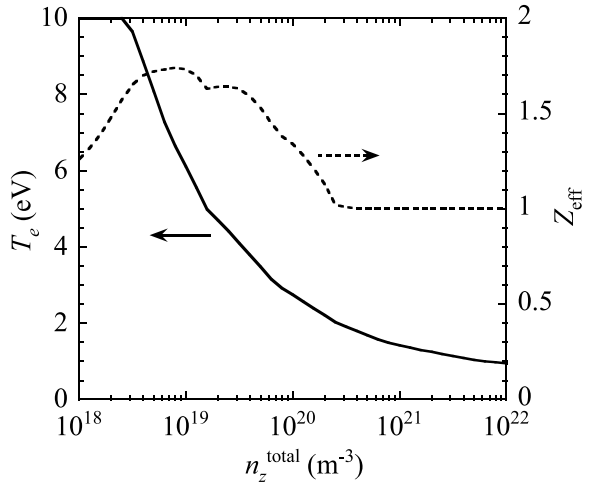

Fig. 6 Two important parameters for the plasma resistivity, T_e (solid line) and Z_{eff} (dashed line) as a function of n_z^{total} calculated with the model. Around $n_z^{total} = 10^{20}\,m^{-3}$, the drops of T_e and Z_{eff} make the change in the plasma resistivity small.

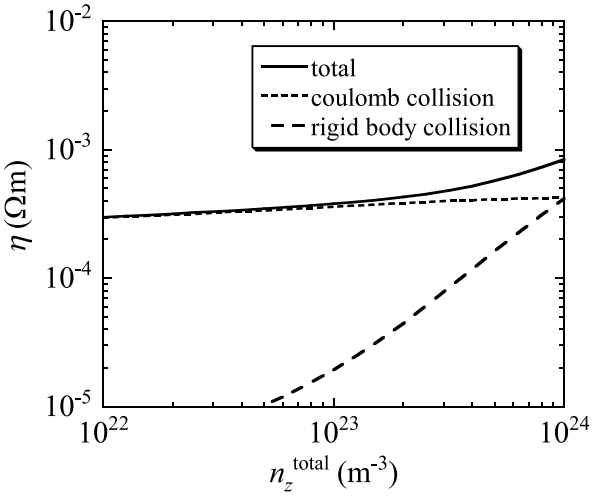

Fig. 7 Contributions to the plasma resistivity (solid line) by the Coulomb collision (short dashed line) and the rigid body collision (long dashed line). Collisions between electrons and neutral particles contribute to the plasma resistivity in $n_z^{total} > 10^{23}\,m^{-3}$.

increase in the amount of impurity can be reproduced reasonably well.

Further improvements of the model in order to increase the accuracy of the evaluation of the current quench time in particular, lie in the following two areas. For a more accurate evaluation of the current decay time, detailed calculations of the time evolutions of the plasma equilibrium and parameters, such as the plasma cross-section area and plasma current, are needed. In order to calculate these evolutions, sophisticated numerical codes such as DINA or TSC must be used, in which an appropriate impurity model should be incorporated to calculate the plasma resistivity (the electron temperature and charge state). The model described in this paper can be easily incorporated into these codes and effectively used in such calculations. Secondly, the employed coronal equilibrium should be expanded to include the non-coronal feature of the impurity radiation and charge state. Inclusion of the radiation opacity effect may also be an important focus for future study.

Acknowledgments

The authors are grateful to Drs. S. Sengoku and Y. Neyatani for their valuable discussions and comments regarding the experimental results from JFT-2M. We are also grateful to Drs. T. Nakano and K. Shimizu for their arrangement in the use of the ADAS code. We acknowledge Dr. T. Ozeki for his continuous encouragement throughout this work.

[1] M. Sugihara *et al.*, *Proc. 20th IAEA Fusion Energy Conf., Vilamoura, Portugal, 2004* (IAEA, Vienna, 2004), IT/P3-29.
[2] K. Masaki *et al.*, J. Nucl. Mater. **220-222**, 390 (1995).
[3] M.N. Rosenbluth, S.V. Putvinski, Nucl. Fusion **37**, 1355 (1997).
[4] R. Yoshino *et al.*, Nucl. Fusion **36**, 295 (1996).
[5] R. Yoshino *et al.*, Nucl. Fusion **37**, 1161 (1997).
[6] V. Lukash *et al.*, Plasma Phys. Control. Fusion **47**, 2077 (2005).
[7] D.G. Whyte *et al.*, J. Nucl. Mater. **313-316**, 1239 (2003).
[8] B.V. Kuteev *et al.*, Nucl. Fusion **35**, 1167 (1995).
[9] M.N. Rosenbluth *et al.*, Nucl. Fusion **37**, 955 (1997).
[10] S.C. Jardin *et al.*, Nucl. Fusion **40**, 923 (2000).
[11] S. Putvinski *et al.*, J. Nucl. Mater. **241-243**, 316 (1997).
[12] Y. Kawano *et al.*, J. Plasma Fusion Res. **81**, 593 (2005).
[13] R. Yoshino *et al.*, Nucl. Fusion **33**, 1599 (1993).
[14] R. Yoshino *et al.*, Nucl. Fusion **39**, 151 (1999).
[15] R. Yoshino, S. Tokuda, Nucl. Fusion **40**, 1293 (2000).
[16] R. Yoshino *et al.*, Plasma Phys. Control. Fusion **39**, 313 (1997).
[17] M. Bakhtiari *et al.*, Nucl. Fusion **45**, 318 (2005).
[18] G. Martin *et al.*, *Proc. 20th IAEA Fusion Energy Conf., Vilamoura, Portugal, 2004* (IAEA, Vienna, 2004), EX/10-6Rc.
[19] S. Sengoku *et al.*, *submitted to* Nucl. Fusion.
[20] R.R. Khayrutdinov, V.E. Lukash, J. Comput. Phys. **109**, 193 (1993).
[21] S.C. Jardin *et al.*, J. Comput. Phys. **66**, 481 (1986).
[22] D.G. Whyte *et al.*, *Proc. 24th Eur. Conf. on Controlled Fusion and Plasma Physics, Berchtesgaden, Germany, 1997* (European Physical Society, Geneva, 1997), Vol. 21A, 1137.
[23] ITER Physics Basis, Nucl. Fusion **39**, 2333 (1999).
[24] T. Shoji *et al.*, JAERI-M83-194 (1983).
[25] NRL plasma formulary, 2000, p. 34.
[26] H.P. Summers, JET-IR06 (1994), http://adas.phys.strath.ac.uk/